geologicaacta

Early Cretaceous Surtseyan volcanoes of the Baño Nuevo Volcanic Complex (Aysén Basin, Eastern Central Patagonian Cordillera, Chile)

A. DEMANT [1] **M. SUÁREZ** [2] **R. DE LA CRUZ** [2] **O. BRUGUIER** [3]

[1] **Pétrologie Magmatique, Université Paul Cézanne (Aix-Marseille)**
Case Courier 441, 13397 Marseille cedex 20, France. E-mail: alain.demant@yahoo.com

[2] **Servicio Nacional de Geología y Minería**
Avenida Santa María 0104, Santiago, Chile

[3] **Laboratoire ICP-MS, UMR, Université de Montpellier II**
Géosciences GPTR AETE 34095 Montpellier cedex 5, France

─┤ A B S T R A C T ├─

Tens of Surtseyan tuff cones are exposed in the Río Coichel valley, between Ñireguao and Estancia Baño Nuevo (Southern Chilean Andes). The Early Cretaceous products of the submarine eruptions rest on, or are interbedded with, shallow marine sandstones of the Hauterivian-early Aptian Apeleg Formation. The Early Cretaceous rocks typically contain large amphibole phenocrysts, clinopyroxene and plagioclase, and have compositions that range from relatively primitive basalts to andesites. The basalts are slightly enriched in LREE and incompatible trace elements. They have low Ti-contents and negative anomalies in Nb and Ta, characteristic of subduction-related magmas. Centimetre-sized amphibole megacrysts and an amphibole-bearing clinopyroxenite xenolith have been found in one of the tuff cones located near Estancia Baño Nuevo. The amphibole megacrysts are pargasite (low Si and Ti, high Mg). The xenolith has diopsidic clinopyroxene with abundant inclusions, and pargasite veins enclosing smaller clinopyroxene neoblasts. Geochemical data show that the megacrysts and the xenolith have the same origin and correspond to underplated igneous bodies crystallized at high pressure.

KEYWORDS | Hydrovolcanism. Patagonian Andes. Aptian. Amphibole. Megacryst. Geochemistry.

INTRODUCTION

Surtseyan eruptions result from shallow level magma-water interaction during the emergence and growth of monogenetic volcanoes through standing water, as shown by the eruptions of Capelinhos in 1957-1958 (Machado et al., 1962; Waters and Fisher, 1971) and Surtsey in 1963-1967 (Thorarinsson et al., 1964). Volcanic eruptions with high water-magma ratios are characterised by dominant fallout *versus* base surge deposits (Kokelaar, 1983, 1986)

and result in the construction of steep tuff cones (Sheridan and Wohletz, 1983; Wohletz and Sheridan, 1983; Moore, 1985). Recent studies have led to a better understanding of the complex physical processes occurring when magma interacts with water, processes that in turn control the mode of fragmentation and depositional facies (Sohn, 1996; Büttner et al., 1999; Cole et al., 2001; Solgevik et al., 2007).

This study focuses on well-exposed and preserved Early Cretaceous tuff cones located in the vicinity of the small town of Ñireguao (Aysén region, Chilean Patagonian Andes). We will first present the geological framework of this peculiar volcanic episode and the characteristics of the hydromagmatic deposits, then follow with the mineral chemistry of the lavas and a suite of a pyroxenite xenolith and amphibole megacrysts from one of the tuff cones. Finally, the geochemistry of the megacrysts and xenolith are compared with that of the lavas, yielding valuable information on the magmatic system at depth and the tectonic regime at the time of eruption.

GEOLOGICAL BACKGROUND

Geological investigations conducted in the Central Patagonian Cordillera during the last decade have established the stratigraphy of the Lower Jurassic to Upper Cretaceous volcanic successions and the interbedded sedimentary formations (Baker et al., 1981; Suárez et al., 1996; 2007; Pankhurst et al., 1998; 2000; De la Cruz et al., 2003; Demant et al., 2007). The oldest volcanic rocks in the studied area (Fig. 1) are represented by the Upper Jurassic-Valanginian Ibáñez Formation (Suárez et al., 2007). A diachronous marine succession of Tithonian to early Aptian age, known as the Coyhaique Group, overlies and locally interfingers with the Ibáñez Formation. From bottom to top, the Coyhaique Group comprises (Fig. 2): i) the shallow marine
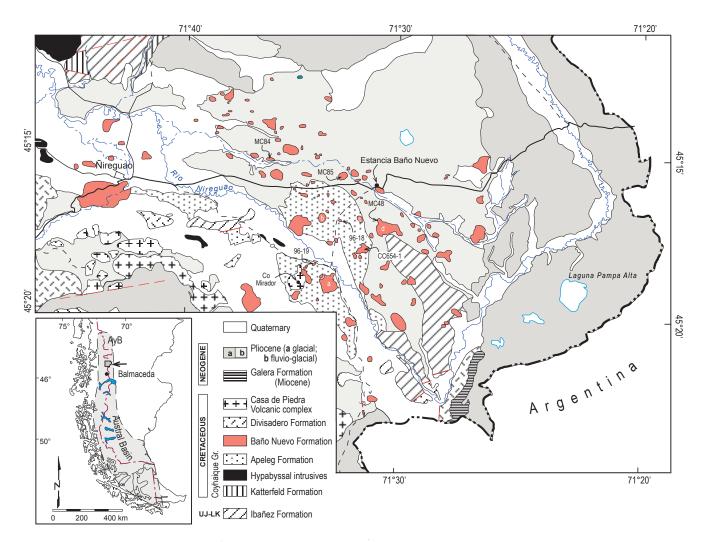

FIGURE 1 | Simplified geological map of the Ñireguao area (modified from Suárez et al., 2007) with location of samples; location of the studied area in the Patagonian region as inset. AyB in the inset, Aysén Basin.
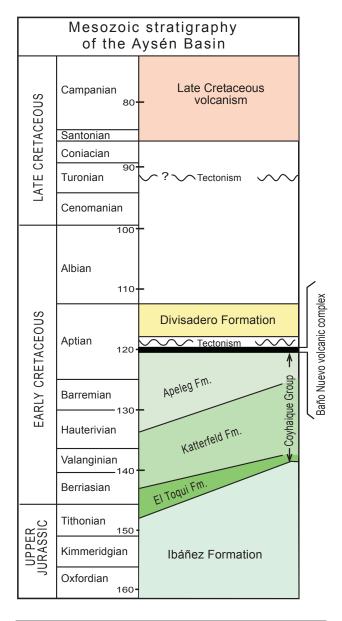
FIGURE 2 | **Mesozoic stratigraphy of the Aysén Basin (modified from De la Cruz et al., 2003 and Suárez et al., 2007).**

Toqui Formation, composed of volcanic sandstones, coral reefs and oyster banks; ii) the Katterfeld Formation mainly formed by black shales representing shelf accumulation; and iii) the Apeleg Formation mainly composed of tidal sandstones (Bell and Suárez, 1997). The Coyhaique Group accumulated in a retroarc basin, the Aysén Basin or Río Mayo Embayment (Ramos and Aguirre-Urreta, 1994; Bell and Suárez, 1997) that represents the northwestern extension of the Austral Basin, better known in the oil-producing region of Magallanes, further south (Biddle et al., 1986; Menichetti et al., 2008; Rossello et al., 2008). An abrupt transition from the Katterfeld to the Apeleg Formation indicates a drastic change from anoxic conditions in a shel-

tered basin to an open marine environment. The Coyhaique Group is unconformably overlain by the volcanic successions of the Divisadero Formation, dated between 118 and 112 Ma (De la Cruz et al., 2003; Pankhurst et al., 2003), and Late Cretaceous volcanic rocks, represented in the area by the rhyolitic and dacitic domes of the Casa de Piedra Volcanic Complex (De la Cruz et al., 2003; Demant et al., 2007). During the Neogene and the Quaternary, the whole area was covered by the Miocene Galera Formation and by glacial and fluvio-glacial deposits accumulated over the eastern foothills of the Andean Cordillera (Fig. 1).

Surtseyan tuff cones formed in shallow water during the waning stages of development of the Aysén Basin. They have been identified in the Río Coichel valley, between Ñireguao and Estancia Baño Nuevo (Fig. 1). Most of the Surtseyan tuff cones form scattered mounds amongst the Neogene successions (Fig. 3A). The products of these submarine eruptions rest on, or are interbedded with, shallow marine sedimentary rocks of the Apeleg Formation. In the south-central part of the area, the Apeleg Formation has been estimated to be 500 m thick (Bell and Suárez, 1997). Shelly mudstones and sandstones occur at the base of the sequence, whereas predominant cross-bedded sandstones in the upper part correspond to sedimentation on a shallow marine shelf (Fig. 3B). Abundant marine fossils preserved in the bedded sandstones date the end of the marine incursion in the Aysén Basin as Hauterivian-early Aptian (Bell and Suárez, 1997). Three Ar/Ar plateau ages obtained on the amphibole-rich lavas of the tuff cones of the Baño Nuevo Volcanic Complex [MC-44: 122.0±0.7 Ma, MC-84: 120.9±0.8 Ma, and MC-86: 121.1±0.7 Ma] indicate an Aptian age. The geochronological data are detailed elsewhere (Suárez et al., 2010).

THE BAÑO NUEVO VOLCANIC FIELD

The Baño Nuevo monogenetic volcano field comprises nearly fifty Surtseyan tuff cones. The best preserved have a diameter of approximately 1km and heights exceeding 100m. They are formed by well stratified pyroclastic material (Fig. 3A) that resulted from successive explosions of varying intensity. The quenched lithic clasts are included in a fine grey to yellowish matrix. The highly vesicular character of the juvenile pyroclasts, the absence of basement fragments and the presence of pellets of muddy Apeleg sediments within the deposits indicate that fragmentation was driven predominantly by magma-water interaction at shallow depth in a marine environment (Sohn, 1996). The good preservation of the Cretaceous landforms emphasizes the weak impact of wave erosion and a quiet marine environment during the volcanic build up (Schmidt and Schmincke, 2002). Crystallization of secondary minerals (calcite and zeolites) and dike intrusions have contributed
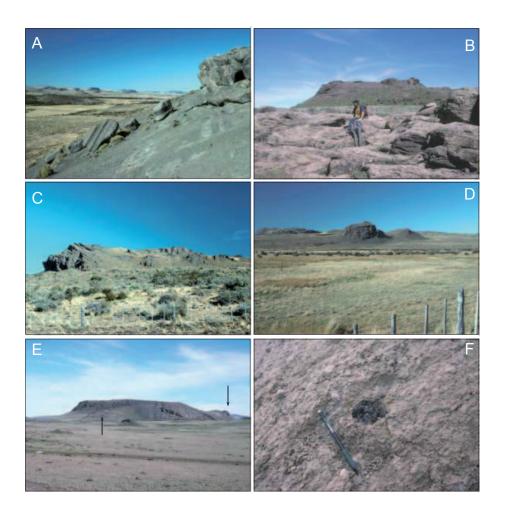
FIGURE 3 | **Some aspects of the Early Cretaceous Baño Nuevo Surtseyan tuff cones. A) general view of the Río Coichel valley with the scattered tuffs cones; in the foreground, aspect of the well-stratified and indurated Surtseyan pyroclastic deposits of the tuff cone seen in (C); B) Surtseyan deposits overlying cross-bedded sandstones of the Apeleg Formation (c in Fig. 1); C) tuff cone located east of Cerro Mirador (a in Fig. 1) showing complex inward-dipping layers; D) partly eroded tuff cones preserving only the near-vent indurated central part (b in Fig. 1); E) massive lava flows filling the crater of a tuff cone (d in Fig. 1): arrows show the zones where Surtseyan deposits are preserved; F) amphibole megacryst in muddy distal facies deposits (sample MC85, Fig. 1); pencil is fifteen centimetres long.**

to the consolidation of the tuffaceous material. In some cones, only the massive central plug and dike system are preserved (Fig. 3D). In a tuff cone located south of Estancia Baño Nuevo (Fig. 1), lava flows were pounded inside the crater before overflowing the crater rim (Fig. 3E). These lava flows could represent the subaerial effusive ending of the eruption when influx of sea water to the vent was prevented, as was exemplified by the eruption of the Surtsey Volcano (Thorarinsson et al., 1964). Complex ventward-dipping and near vertical-dipping layers in the tuff cone located east of Cerro Mirador (Fig. 3C) indicate synvolcanic ring-faulting and changing vent activity (Solgevik et al., 2007). In the wet environment that characterises Surtseyan activity, remobilization of non-welded hyaloclastites by slumping on the outer flanks of the emergent tuff cones is an important process that generates fine-grained distal deposits (Sohn, 1996). The deposit that includes the amphibole megacrysts (sample MC85, Fig. 1) is a good example of such distal lithofacies (Fig. 3F). A distinct coarse breccia facies has been observed south of Ñireguao (Fig. 1) containing glassy and non-vesicular juvenile clasts (1 cm to up to > 2 m in size) with abundant plagioclase microlites. Lenses of sandy material are embedded in the breccia. This coarser facies has been interpreted as being due to

the shattering of the outer margin of a viscous lava dome during its subaquatic emplacement (Smellie et al., 1998; Schmidt and Schmincke, 2002). Finely laminated calcareous deposits are observed among the volcanic clasts. As limestones are not known in the Apeleg Formation, these deposits could represent either algal coating related to hydrothermal activity or lacustrine facies.

In summary, both fossil associations in the Apeleg sandstones and the characteristics of the volcanic tephra show that the Baño Nuevo tuff cones were formed in shallow water during the regression of the Aysén Basin in Early Cretaceous time.

ANALYTICAL METHODS

Rock samples were ground first in a steel jaw crusher and then finely powdered in an agate grinder. Major elements were analyzed by inductively-coupled-plasma-atomic-emission spectrometry (ICP-AES); trace elements were obtained by inductively-coupled-plasma-mass spectrometry (ICP-MS). Major element compositions of the minerals were determined using a Cameca SX-100 elec-

tron microprobe fitted with five wavelength dispersive spectrometers at the "Service Commun Microsonde Sud" (University of Montpellier II). The standard operating conditions included an accelerating voltage of 20 kV, a beam current of 10 nA and integrated counting times ranging from 20 to 30 s.

Laser ablation (LA-) ICP-MS analyses were performed at the Géosciences Laboratory (University of Montpellier II) using a single collector double-focussing sector field element XR (Extended Range) ICP-MS coupled with a Geolas (Microlas) automated platform housing an ArF Compex 102 laser from LambdaPhysik generating 15 ns duration pulses of radiation at a wavelength of 193 nm. After microprobe analysis, thick rock sections (~ 150 μm thick) were cleaned with alcohol, dried under nitrogen and introduced into the ablation cell at least half an hour before starting the measurements. Ablation experiments were conducted in an ablation cell of ca. 30 cm^3 in an He atmosphere, which enhances sensitivity and reduces inter-element fractionation (Gunther and Heinrich, 1999). The helium gas stream and particles from the sample were then mixed with Ar before entering the plasma. Data were acquired in the fast E-scan mode at low resolution (M/ΔM=300). Signals were measured in Time Resolved Acquisition (TRA), devoting 2 minutes for the blank and 1 minute for measurement of the analytes. The laser was fired using an energy density of 15 J cm^{-2} at a frequency of 5 Hz and using a spot size of 77 μm. Oxide level, measured using the ThO/Th ratio, was below 0.7%. ^{43}Ca was used as an internal standard and analyte concentrations were calibrated against the NIST 612 rhy-

olitic glass using the values given in Pearce et al. (1997). Data were subsequently reduced using the GLITTER software (Achterbergh et al., 2001) by carefully inspecting the time-resolved analysis to check for lack of heterogeneities (inclusions or fractures) in the analyzed volume.

THE BAÑO NUEVO VOLCANIC ROCKS

Petrological and geochemical features

Magmas involved in the Early Cretaceous Surtseyan eruptions are distinguished by the abundance of large amphibole phenocrysts associated with clinopyroxene and plagioclase. This primary mineral assemblage is well-preserved only in the massive lava flows or dikes. A dike (sample 96-19) with a subophitic texture presents the only occurrence of fresh olivine. Massive rocks in the central part of some edifices (*i.e.*, MC82, Fig. 1) are coarse-grained plagioclase- and amphibole-rich lavas. As a result of slower cooling, these rocks have been more affected by late hydrothermal alteration. Calcite and zeolites are abundant secondary phases in the matrix or as vein fillings. In the tuff cone sequences moderately to highly vesicular glassy fragments coexist; the latter have amygdaloidal textures, with calcite and chlorite filling the vesicles.

The Early Cretaceous rocks have a large range of compositions (Table 1), from relatively primitive basalts with mg# [molar $100xMg/(Mg + Fe_{total})$] between 62 and 67, to basaltic andesites and andesites (~ 61 wt% SiO_2,

TABLE 1 | **Bulk rock chemical compositions of the Baño Nuevo lavas. Analyses performed at: * University of Aix-Marseille, ° Centre de Recherches Pétrographiques et Géochimiques (CRPG) of Nancy; + Servicio Nacional de Geología y Minería (SERNAGEOMIN) Santiago.**

	96-18*	MC14[+]	MC84[+]	96-19*	MC85[+]	MC82[+]	96-25*	CC654-1°	MC44[+]	MC86-1[+]	MC86[+]	MC46[+]
SiO_2	45.39	46.17	46.45	46.78	48.38	48.55	49.96	50.28	50.84	53.56	54.95	60.57
TiO_2	1.40	1.26	1.30	1.26	1.05	1.19	1.07	1.02	0.92	0.77	0.79	0.84
Al_2O_3	16.51	19.46	17.38	18.00	18.01	16.82	16.03	18.35	18.80	17.52	17.46	18.26
Fe_2O_3	4.08	11.75	11.05	3.08	10.20	9.34	3.48	7.28	8.84	6.82	7.01	5.54
FeO	6.01			7.53			4.85					
MnO	0.13	0.14	0.17	0.20	0.19	0.21	0.21	0.44	0.26	0.18	0.20	0.10
MgO	8.47	4.42	5.66	7.93	4.52	5.93	7.60	4.08	3.41	2.47	2.43	2.62
CaO	8.00	10.68	7.90	9.61	7.52	7.84	8.46	9.15	8.41	7.62	7.77	5.41
Na_2O	2.99	2.82	4.75	2.89	4.47	3.81	2.48	3.85	3.79	3.30	3.39	4.37
K_2O	1.62	1.06	1.42	0.69	1.71	1.94	1.71	1.71	1.93	2.08	2.21	1.27
P_2O_5	0.25	0.20	0.26	0.29	0.52	0.43	0.29	0.38	0.40	0.32	0.32	0.22
LOI / H_2O^+	4.10	1.93	3.44	1.47	3.23	3.81	3.18	3.25	2.31	5.13	3.31	0.50
H_2O^-	0.47			0.11			0.57					
Total	99.42	99.88	99.78	99.84	99.80	99.87	99.89	99.79	99.90	99.76	99.84	99.71
mg#	64.94	46.96	54.65	61.98	51.04	59.90	66.85	56.87	47.59	46.00	44.92	52.67

sample MC46). Major element contents are highly variable which is probably related to the common post-magmatic alteration in such subaquatic environments. On the total alkalis *vs* silica diagram (Fig. 4A), some basalts plot in the field of alkaline lavas. MgO contents are highly variable in the basaltic lavas but globally decrease with increasing SiO_2 (Fig. 4B), suggesting an evolution by fractional crystallization. Titanium is low and alumina high, a common feature in arc volcanism. The trace element concentration of four basaltic samples (Table 2) shows that the Rare Earth Element (REE) patterns (Fig. 5A) are characterised by a slight enrichment in Light Rare Earth Elements [LREE, $(La/Sm)_n$ ranging from 2.6 to 3.3], an absence of Eu anomalies, and flat Heavy Rare Earth Elements [HREE, $(Gd/Yb)_n \sim 1.6$]. Sample 96-19 from the dike is less enriched in LREE [$(La/Yb)_{n^\circ}= 3.7$ instead of 6.4 to 9]. On the multi-elements diagram, basalts also show similar patterns with a regular increase toward the most incompatible elements and negative anomalies in High Field Strength Elements (HFSE), well-pronounced for Nb-Ta and slightly less for Zr-Hf (Fig. 5B). On this same diagram, sample 96-19 appears
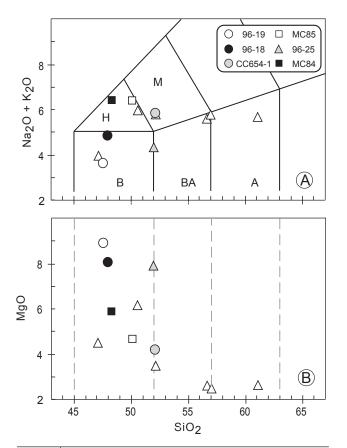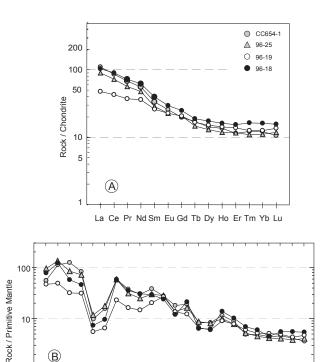
less enriched in incompatible elements (from Sr to Rb) than the rest.

Mineral compositions and textural relationship

Fresh olivine in sample 96-19 is present as small euhedral phenocrysts (< 0.5 mm) with tiny inclusions of green spinel and shows minor alteration to chlorite. Olivine displays a wide compositional range from Fo_{83} to Fo_{58} (Fig. 6D). Amphibole (up to 6 mm in size, Fig. 7F) has low Ti (<0.50 atom per formula unit, afu), (Na + K) afu > 0.50 and mg# ranging from 61 to 77. Slight differences in composition are observed between samples (Table 3; Fig. 6A). Amphibole from sample 96-18 has the highest mg# and corresponds to pargasite (classification of Leake et al., 1997) whereas MC48 and MC84 amphiboles are less magnesian. Clinopyroxene (Table 3; Fig. 6B) is highly calcic and diopsidic (Morimoto et al., 1988) forming zoned euhedral phenocrysts in the lavas but being a late crystallizing phase in the subophitic-textured dike (96-19). Clinopyroxene and amphibole phenocrysts in sample MC84 exhibit reverse zoning, with Mg

FIGURE 4 | **A) Total alkalis vs silica (TAS) diagram (Le Bas et al., 1986).** B, basalts; BA, basaltic andesites; A, andesites; H, hawaiite; M, mugearite. B) MgO *vs* silica diagram for the Baño Nuevo lavas.

TABLE 2 | **Trace element compositions (ppm) of selected samples of the Baño Nuevo lavas. Analyses obtained by ICP-MS at the University of Montpellier.**

	96-18	96-19	96-25	CC654-1
Rb	49.8	29.8	60.4	36.2
Ba	858	343	940	796
Sr	508	569	599	589
Nb	5.29	3.99	8.36	6.93
Zr	71	74	97	94
Y	20.5	23.2	19.1	20
Pb	5.47	3.79	5.59	7.1
Th	4.95	2.74	7.23	10.58
Ta	0.4	0.27	0.72	0.64
Hf	1.95	1.85	2.5	2.59
U	0.97	0.66	1.51	1.73
La	24.52	11.24	21.34	26.02
Ce	55.00	26.23	44.61	52.82
Pr	6.91	3.56	5.36	6.47
Nd	28.86	16.74	22.11	25.89
Sm	6.10	4.00	4.40	5.11
Eu	1.72	1.32	1.32	1.48
Gd	5.13	4.22	4.21	4.06
Tb	0.71	0.63	0.55	0.64
Dy	4.41	3.81	3.31	3.62
Ho	0.91	0.81	0.67	0.76
Er	2.56	2.28	1.91	1.89
Tm	0.42	0.32	0.28	0.31
Yb	2.75	2.14	1.89	2.06
Lu	0.40	0.35	0.30	0.27

increasing toward the rim of the crystals. The presence of sieve-textured plagioclases with labradorite cores is additional evidence that magma mixing occurred. Plagioclase forms laths embedded in clinopyroxene in the dike and euhedral phenocrysts in the lava flows. Its composition is mainly bytownitic but more sodic compositions were also found (Fig. 6C). Plagioclase is strongly altered and partly replaced by calcite, albite, zeolite and/or sericite. The original glassy matrix is transformed into a fine grained assemblage of Fe-Ti oxides (magnetite or titanomagnetite), highly-pleochroic Ti-rich biotite (~ 6 wt % TiO_2), chlorite and zeolites. Several kinds of zeolites have been identified by their optical properties and chemistry (Tschernich, 1992). Vesicles in the pyroclastic material (*e.g.*, sample MC48) are first filled by analcite and then by prismatic thomsonite (Ca-Na zeolite). In other vesicles, a brownish radial mesolite is intimately associated with thomsonite.

MEGACRYSTS AND PYROXENITE XENOLITH

Amphibole megacrysts

Centimetre-sized amphibole megacrysts have been found in the pyroclastites of a tuff cone located near Estancia Baño Nuevo (MC85, Figs. 1 and 3F). Disequilibrium of the megacrysts with respect to the host is evidenced by the fact that they are partially (Fig. 7A) or totally (Fig. 7B) engulfed by glassy vesicular lava. Amphiboles are compositionally homogeneous (Table 4) which is common in the megacrysts (Gutmann, 1977; Irving and Frey, 1984; Righter and Carmichael, 1993; Shaw and Eyzaguirre, 2000). They correspond to pargasite (Fig. 8A) with molar Ti < 0.50, low Si, high mg# (75-78), similar percentages in sodium and potassium (~ 1.84 and 1.89 respectively) and very low Cr content. Arrays of elongated (30-50 μm) opaque inclusions (Fig. 7C), qualitatively determined by electron microprobe as Fe-sulphide (pyrrhotite), are observed in some amphibole megacrysts and may represent droplets of immiscible sulphide liquid incorporated into the growing silicates (Peterson and Francis, 1977; Szabó and Bodnar, 1995; Shaw, 1997; Zajacz and Szabó, 2003; Woodland and Jugo, 2007).

Pyroxenite xenolith

A pyroxenite xenolith (7 cm maximum size) was found in the same tuff cone together with the megacrysts. Two generations of clinopyroxene were identified in this xenolith (Fig. 7D): 1) large subhedral crystals with undulose extinction and simple twinning containing rounded or elongated sulfide droplets and trails of inclusions;
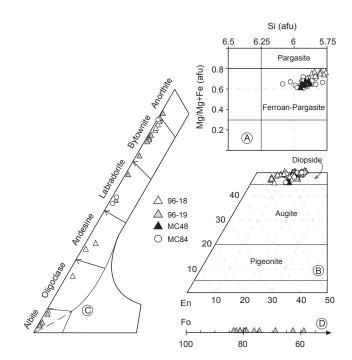

FIGURE 6 | **Mineral chemistry of the Baño Nuevo lavas. Classification based on Leake et al. (1997) for amphiboles A) and Morimoto et al. (1988) for pyroxenes B). C) Compositions of plagioclases and D) of olivines.**
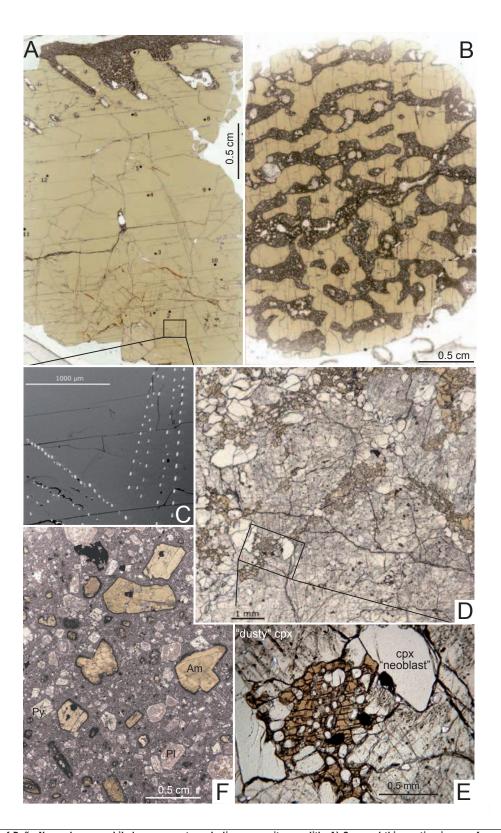
FIGURE 7 | **Images of Baño Nuevo lava, amphibole megacrysts and clinopyroxenite xenolith. A) Scanned thin-section image of amphibole MC85am1 megacryst; small black dots show the position of microprobe analyses. Note the engulfed contour of the crystal in the upper part of the photo. B) Scanned thin-section image of a "vuggy" amphibole megacryst (MC85am2). C) Back-scattered electron image showing trails of sulphide blobs; this image corresponds to the delimited zone on the scanned thin-section image. D) Scanned thin-section image of the pyroxenite xenolith showing the primary "dusty" clinopyroxenes invaded by veins of pargasitic amphibole and clear clinopyroxene "neoblasts". E) Detail of an amphibole vein showing poikilitic pargasite enclosing small clinopyroxene "neoblasts". F) Scanned thin-section image of an amphibole-rich lava (sample MC84) representative of the Baño Nuevo lavas.**

TABLE 3 | **Representative microprobe analyses of amphibole and pyroxene phenocrysts of the Baño Nuevo lavas.**

Amphibole

Sample n°	96-18			MC48				MC84			
Analysis	211	212	216	45	42	49	39	62	81	92	109
SiO$_2$	39.07	39.63	39.33	39.70	39.64	39.44	39.57	39.79	40.45	40.83	39.70
Al$_2$O$_3$	15.58	15.38	15.26	15.48	14.54	15.05	14.76	15.41	14.03	13.67	14.56
FeO*	8.11	8.59	9.16	10.62	11.76	12.22	12.95	9.62	11.31	12.24	13.16
MnO	0.09	0.12	0.07	0.12	0.16	0.15	0.19	0.09	0.17	0.17	0.25
MgO	15.12	14.68	14.24	12.79	12.50	12.04	11.55	13.63	12.99	12.98	11.69
CaO	12.91	12.36	12.39	12.23	12.07	12.00	11.85	12.39	11.84	11.75	11.88
Na$_2$O	1.92	2.02	2.11	1.90	2.04	1.94	2.03	1.88	2.19	2.23	2.10
K$_2$O	2.17	1.84	2.00	1.62	1.40	1.52	1.49	1.49	1.17	0.92	1.26
TiO$_2$	2.49	2.19	2.30	2.38	2.69	2.59	2.59	2.64	2.66	2.27	2.27
Cr$_2$O$_3$	0.13	0.05	0.25	0.03	0.03	0.00	0.03	0.00	0.11	0.02	0.04
Total	97.60	96.86	97.13	96.87	96.83	96.94	97.02	96.93	96.91	97.07	96.90
Mg#	77.03	75.37	73.56	68.28	65.51	63.78	61.41	71.71	67.19	65.47	61.36

Clinopyroxene

Sample n°	96-18				96-19		MC48			MC84		
Analysis	194	234	233	237	119	120	32	31	47	87	84	98
SiO$_2$	51.22	49.46	47.97	47.69	49.82	47.86	48.44	48.78	46.27	50.83	47.88	46.17
Al$_2$O$_3$	3.23	6.06	7.53	7.32	3.16	4.97	6.72	6.34	7.95	3.39	6.66	7.97
FeO*	3.63	4.41	5.16	5.65	7.68	8.67	6.35	7.38	9.21	7.27	8.50	9.77
MnO	0.11	0.13	0.02	0.08	0.14	0.26	0.13	0.15	0.21	0.24	0.22	0.25
MgO	16.79	14.75	14.16	13.59	14.75	12.77	13.28	12.74	11.23	14.41	12.51	10.82
CaO	23.33	23.12	22.95	22.74	22.64	22.67	22.81	22.67	22.42	22.05	21.95	22.81
Na$_2$O	0.21	1.10	0.41	0.36	0.26	0.40	0.22	0.29	0.33	0.24	0.29	0.38
TiO$_2$	0.32	0.63	0.98	1.01	0.95	1.65	1.03	0.93	1.20	0.65	1.34	1.23
Cr$_2$O$_3$	0.61	0.34	0.03	0.10	0.06	0.00	0.08	0.00	0.00	0.04	0.02	0.01
Total	99.45	100.01	99.19	98.53	99.47	99.24	99.06	99.28	98.83	99.13	99.38	99.41
Wo	47.03	49.00	49.15	49.31	45.96	47.82	49.22	48.99	49.39	45.97	47.55	49.93
En	47.08	43.49	42.19	40.99	41.65	37.47	39.86	38.30	34.41	41.80	37.70	32.95
Fs	5.89	7.51	8.66	9.70	12.39	14.71	10.92	12.71	16.20	12.23	14.75	17.12

TABLE 4 | **Mineral chemistry of amphibole megacrysts and the xenolith. MC85am1 and MC85am2 correspond to the thin sections seen in Figure 7A and 7B, respectively. MC85am3 is a smaller amphibole megacryst that encloses clinopyroxene (analyses MC85am3 cpx). Analyses of amphibole veins cross-cutting the clinopyroxene xenolith (MC85xe) are also given. For pyroxene, the averages of the "dusty" primary clinopyroxene and of the clear "neoblasts" are reported. The "dusty cpx2" corresponds to zones in the primary clinopyroxene with fewer inclusions. n: number of analyses used to calculate the averages and the standard deviation (σ).**

Amphibole

	Megacrysts						Xenolith veins	
	MC85am1		MC85am2		MC85am3		MC85xe	
	n=12	σ	n=26	σ	n=20	σ	n=13	σ
SiO$_2$	41.12	0.19	41.67	0.32	41.26	0.37	40.45	0.53
Al$_2$O$_3$	14.73	0.09	14.85	0.22	15.02	0.16	15.39	0.35
FeO*	8.45	0.09	7.66	0.06	8.68	0.19	7.96	0.11
MnO	0.10	0.01	0.08	0.01	0.10	0.01	0.08	0.01
MgO	14.72	0.12	15.40	0.13	14.69	0.20	14.73	0.24
CaO	11.80	0.03	12.05	0.06	12.05	0.04	11.91	0.08
Na$_2$O	1.89	0.05	1.83	0.07	1.86	0.05	1.78	0.07
K$_2$O	1.78	0.03	1.96	0.08	1.81	0.13	2.01	0.14
TiO$_2$	2.03	0.05	1.96	0.06	2.09	0.05	2.23	0.18
Cr$_2$O$_3$	0.02	0.02	0.20	0.03	0.06	0.02	0.14	0.08
Total	96.64		97.66		97.62		96.68	

Clinopyroxene

	MC85xe						MC85am3	
	"dusty cpx1"		"dusty cpx2"		"neoblast"		cpx	
	n=15	σ	n=13	σ	n=7	σ	n=9	σ
SiO$_2$	49.13	0.8	49.47	0.63	49.27	0.46	49.89	0.24
Al$_2$O$_3$	6.48	1.03	6.11	0.67	6.28	0.47	6.09	0.16
FeO*	5.43	0.18	5.52	0.29	5.65	0.08	6.16	0.07
MnO	0.11	0.01	0.12	0.01	0.13	0.01	0.14	0.02
MgO	14.28	0.47	14.40	0.48	14.18	0.26	14.13	0.13
CaO	22.02	0.08	21.99	0.08	21.99	0.21	22.58	0.11
Na$_2$O	0.35	0.02	0.35	0.03	0.34	0.04	0.33	0.02
TiO$_2$	0.93	0.18	0.81	0.13	0.79	0.09	0.79	0.04
Cr$_2$O$_3$	0.16	0.04	0.13	0.06	0.15	0.04	0.03	0.01
Total	98.89		98.90		98.78		100.14	

2) smaller clear subhedral grains (neoblasts) spatially related to amphibole in veins invading the primary "dusty" pyroxenes (Fig. 7D and 7E). The latter have high mg# (~82) and are compositionally homogeneous corresponding to Cr-poor diopside (Cr$_2$O$_3$ < 0.25 wt %), rich in Ca and Mg (Wo47 En43 Fs9) and low in Ti and Na (Table 4). Clinopyroxene neoblasts and crystals included in some of the amphibole megacrysts (MC85am3) have the same composition (Table 4; Fig. 8B) and correspond to local recrystallisation of the clinopyroxenite xenolith. Carbonates are also present in the xenolith. Carbonates coexisting with silicates normally suffer decarbonation upon decompression (Frezzotti et al., 2002). Calcite appears in the vesicles of the amygdaloidal lava enclosing the xenolith, suggesting that carbonates probably formed during post-eruptive processes at the surface.

Trace element contents

Trace element contents have been determined by laser ablation (LA-) ICP-MS analysis. Amphibole megacrysts have a similar composition to the amphibole from hydrous veins in the clinopyroxenite (Table 5). Both display upward-concave normalized REE patterns, and low LREE (Fig. 9). On an extended primitive mantle normalized trace element diagram (not shown), amphibole patterns are characterised by prominent spikes in K, Ba and Rb and negative anomalies in Th, U, Zr and Hf. Trace element abundances in pyroxene are characterised by strong depletions in Rb, Ba, K, Nb and Ta compared to amphibole. Clinopyroxene from the xenolith presents the same REE patterns as the amphibole megacrysts, although its REE concentrations are slightly lower (Fig. 9).

DISCUSSION

Origin of amphibole megacrysts and clinopyroxenite

Megacrysts commonly occur in alkali basalts together with mafic and ultramafic xenoliths (*e.g.*, Frey and Prinz, 1978; Irving and Frey, 1984; Wilshire et al., 1991; Shaw and Eyzaguirre, 2000) but are much rarer in calc-alkaline lavas. Large unzoned megacrysts did not crystallize from their host lava but rather correspond to xenocrysts formed at depth (Righter and Carmichael, 1993; Shaw and Eyzaguirre, 2000). The size of megacrysts and their homogeneous composition require slow crystallization and a long residence time at high temperature. Such physical conditions prevail when voluminous batches of magma are trapped in the subcontinental mantle. Moreover, the overall geochemical features of the Baño Nuevo megacrysts, in particular the depletion in Nb, match those of amphiboles generated in the mantle wedge above subduction zones (S-Amph of Coltorti et al., 2007).

Clinopyroxenite xenoliths, on the other hand, are widely considered as cumulates of fractionating mantle magmas that could occur at various depths in the mantle lithosphere (e.g., Litasov et al., 2000; Shaw and Eyzaguirre, 2000). The geochemical similarities between 1) amphibole megacrysts and vein amphibole from the clinopyroxenite and 2) clinopyroxene included in amphibole megacrysts and pyroxene from the clinopyroxenite, suggest that both megacrysts and the xenolith come from a common mantle source. The poikilitic association of amphibole and pyroxene in the veins suggests that amphibole corresponds to a late metasomatic event. This event also formed high-pressure pegmatite-like pockets of amphibole that might be the source of the amphibole megacrysts.

A question arises about the composition of the melt that formed the clinopyroxenite and the megacrysts. The parent magma composition can be calculated from the amphibole and clinopyroxene REE and trace element data (Shaw and Eyzaguirre, 2000; Woodland and Jugo, 2007) using available mineral/liquid partition coefficients (Zack et al., 1997). The pattern of the parent magma calculated using the clinopyroxene composition from the xenolith falls in the field of the Baño Nuevo lavas (Fig. 9) whereas that calculated from the amphibole megacrysts is slightly more enriched suggesting that amphibole crystallized from a more differentiated melt. Moreover, it was S-saturated leading to the formation of sulfide inclusions. To better constrain the composition of the parental melt and the depth at which melt formed in the mantle, an accurate study of the fluid and melt inclusions present in the "primary" clinopyroxene of the xenolith and amphibole megacrysts would be necessary. Amphibole is uncommon in calc-alkaline basaltic lavas; its abundance in the Baño Nuevo rocks reflects a high
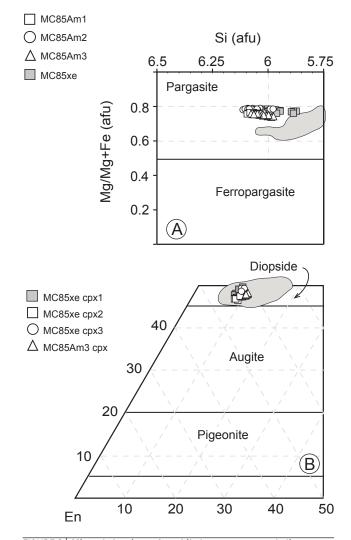

FIGURE 8 | **Mineral chemistry of amphibole megacrysts and clinopyroxenite xenolith. Grey fields correspond to the composition of phenocrysts shown in Figure 6.**

volatile content, a possible consequence of a low degree of partial melting.

Geodynamic implications

Xenoliths and megacrysts provide unique information on the nature of the mantle beneath volcanic systems as well as constraints on the ascent mechanism of the host lava. Clinopyroxene cumulate xenoliths are samples of probable voluminous igneous bodies which did not reach the surface but accumulated in the subcontinental lithospheric mantle where they crystallized slowly. Similarities in mineralogy and trace elements between the clinopyroxenite and the Baño Nuevo rocks indicate that they were derived from a similar mantle source. One can speculate that the intrusion of the underplated melts shortly preceded volcanic activity. Amphibole megacrysts are vuggy but no

TABLE 5 | **In situ LA-ICP-MS analyses of amphibole megacryst MC85am1 and vein amphibole (MC85xe), "dusty" primary clinopyroxene and clear "neoblasts" from the clinopyroxenite xenolith (MC85xe). n: number of analyses used to calculate the averages and the standard deviation (σ).**

	Amphibole				Pyroxene			
	MC85am1		MC85xe		MC85xe			
	megacryst		Xenolith veins		"dusty cpx"		"neoblast"	
n	7	σ	5	σ	7	σ	3	σ
Rb	11.85	0.18	13.01	0.67	0.10	0.14	0.04	0.04
Ba	335	2.34	365	15.48	1.15	1.9	0.68	1.31
Sr	267	4.10	266	9.84	46.8	2.8	47.8	2.41
Nb	1.1	0.08	1.6	0.15	0.05	0.02	0.04	0.01
Zr	22.7	6.56	18.6	7.94	18.6	9.2	11.0	1.67
Y	12.6	0.23	11.4	0.73	9.20	0.67	9.07	0.29
Th	0.07	0.01	0.27	0.38	0.12	0.07	0.07	0.02
Ta	0.10	0.02	0.16	0.03	0.02	0.01	0.01	0.01
Hf	0.81	0.17	0.75	0.11	0.68	0.13	0.69	0.04
U	0.01		0.02		0.04		0.03	
La	2.06	0.08	2.05	0.25	1.16	0.14	1.17	0.06
Ce	7.59	0.29	7.11	0.58	4.53	0.48	4.62	0.30
Pr	1.44	0.04	1.35	0.13	0.92	0.11	0.92	0.07
Nd	8.61	0.13	7.63	0.51	5.60	0.82	5.58	0.18
Sm	2.81	0.06	2.45	0.11	1.99	0.17	1.91	0.04
Eu	0.90	0.02	0.82	0.03	0.64	0.04	0.62	0.03
Gd	3.04	0.06	2.72	0.12	2.09	0.11	2.09	0.06
Tb	0.42	0.01	0.39	0.03	0.33	0.03	0.32	0.00
Dy	2.67	0.12	2.45	0.18	2.07	0.08	2.03	0.08
Ho	0.51	0.02	0.47	0.03	0.40	0.03	0.38	0.02
Er	1.38	0.05	1.22	0.10	1.04	0.08	0.99	0.04
Tm	0.18	0.01	0.16	0.01	0.13	0.02	0.13	0.00
Yb	1.05	0.07	0.98	0.04	0.88	0.07	0.81	0.03
Lu	0.14	0.01	0.13	0.01	0.11	0.01	0.11	0.00

FIGURE 9 | **Chondrite normalized REE patterns of amphibole megacrysts, vein amphibole and pyroxenes from the xenolith. Grey field represents the pattern of whole rock samples shown in Figure 5. Normalizing values are from Sun and McDonough (1989). Patterns of parental magmas of amphibole megacryst (pm Amp) and clinopyroxenite (pm Cpx) were calculated using partition coefficients taken from Zack et al. (1997).**

reaction is observed at the contact between amphibole and the host magma (Fig. 7A, B). This indicates that 1) mega–crysts were dissolved and partially melted by the host magma at depth but 2) very high ascent rates prevented further equilibration with the liquid en route to the surface. High ascent rates imply easier access to the surface for the magmas and characterise extensional regimes. At about 121 Ma, numerous tuff cones were emplaced during the last stages of the marine back-arc Aysén Basin, preceding its inversion and a contractional tectonic event locally observed (Suárez and De la Cruz, 2000; Iannizzotto et al., 2004). This shallow marine volcanic episode was followed by the subaerial subduction-related volcanism of the Divisadero Formation that started approximately 3-5 Ma later.

SUMMARY

The study of the Aptian (121 Ma) Baño Nuevo Volcanic Complex provides direct evidence concerning its origin and mode of emplacement.
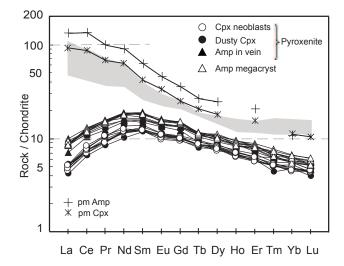
Field observations show that this volcanic complex corresponds to a succession of Surtseyan eruptions that occurred during the emerging stage of volcanic islands in an epicontinental sea during the sedimentation of the clastic Apeleg Formation.

The Baño Nuevo lavas have calc-alcaline affinities with compositions ranging from relatively primitive basalts to andesites. A prominent feature of these lavas is the abundance of large amphibole phenocrysts, reflecting an origin by low degree of partial melting.

The occurrence of amphibole megacrysts and a clinopyroxenite xenolith indicate that slow cooling mafic melts were trapped in the lithospheric mantle before volcanic activity began.

Similarity between the trace element characteristics of the xenolith and megacrysts and those of the host lava indicates a similar mantle source and suggests that intrusion of the melt bodies shortly pre-dated the volcanic activity.

The presence of megacrysts and the xenolith are evidence of a rapid ascent of the host lava; their easy access to the surface suggests the existence of deep faults serving as conduits for the rising magmas at 121 Ma.

REFERENCES

Van Achterbergh, E., Ryan, C.G., Jackson, S.E., Griffin, W., 2001. Data reduction software for LA-ICP-MS. In: Sylvester, P. (ed.). Laser Ablation ICP-MS in the Earth Science. Mineralogical Association of Canada, 29, 239-243.

Baker, P.E., Rea, W.J., Skarmeta, J., Caminos, R., Rex, D.C., 1981. Igneous history of the Andean cordillera and Patagonian plateau around latitude 46°S. Philosophical Transactions of the Royal Society, A303, 105-149.

Bell, C.M., Suárez, M., 1997. The Lower Cretaceous Apeleg Formation of the Aisén basin, southern Chile. Tidal sandbar deposits of an epicontinental sea. Revista Geológica de Chile, 24, 203-226.

Biddle, K.T., Uliana, M.A., Mitchum, R.M.Jr., Fitzgerald, M.G., Wright, R.C., 1986. The stratigraphic and structural evolution of the central and eastern Magallanes basin, southern South America. In: Allen, P.A., Homewood, P. (eds.). Foreland Basins. International association of sedimentologists Special publications, Oxford (United Kingdom), Blackwell Scientific Publications, 8, 41-61.

Büttner, R., Dellino, P., Zimanowski, B., 1999. Identifying magma-water interaction from the surface features of ash particles. Nature, 104, 688-690.

Cole, P.D., Guest, J.E., Duncan, A.M., Pacheco, J-M., 2001. Capelinhos 1957-1958, Faial, Azores: deposits formed by an emergent Surtseyan eruption. Bulletin de Volcanologie, 63, 204-220.

Coltorti, M., Bonadiman, C., Faccini, B., Grégoire, M., O'Reilly, S.Y., Powell, W., 2007. Amphibols from suprasubduction and intraplate lithospheric mantle. Lithos, 99, 68-84.

De la Cruz, R., Suárez, M., Belmar, M., Quiroz, D., Bell, M., 2003. Geología del área Coyhaique-Balmaceda, Región de Aisén del General Carlos Ibáñez del Campo. Servicio Nacional de Geología y Minería, Carta Geológica de Chile, Serie Geología Básica 1:100.000, 80, 40pp.

Demant, A., Suárez, M., De la Cruz, R., 2007. Geochronology and petrochemistry of Late Cretaceous - (?) Paleogene volcanic sequences from the eastern central Patagonian Cordillera (45°-45°40'S). Revista Geológica de Chile, 34, 3-21.

Frey, F.A., Prinz, M., 1978. Ultramafic inclusions from San Carlos, Arizona: Petrologic and geochemical data bearing on their petrogenesis. Earth and Planetary Science Letters, 38, 129-176.

Frezzotti, M-L., Touret, J.L.R., Neumann, E-R., 2002. Ephemeral carbonate melts in the upper mantle: carbonate-silicate immiscibility in microveins and inclusions within spinel peridotite xenoliths, La Gomera, Canary Islands. European Journal of Mineralogy, 14, 891-904.

Günther, D., Heinrich, C.A., 1999. Enhanced sensitivity in LA-ICP-MS using helium-argon mixtures as aerosol carrier. Journal of Analytical Atomic Spectrometry, 14, 1369-1374.

Gutmann, J.T., 1977. Textures and genesis of phenocrysts and megacrysts in basaltic lavas from the Pinacate field. American Journal of Science, 277, 833-861.

Iannizzotto, N.F., Folguera, A., Leal, P.R., Iaffa, D., 2004. Control tectónico de las secuencias volcaniclásticas neocomianas y paleogeografía en la zona del Lake La Plata (45ºS). Sector interno de la faja plegada y corrida de los Lakes La Plata y Fontana. Revista de la Asociación Geológica Argentina, 59(4), 1-21.

Irving, A.J., Frey, F.A., 1984. Trace element abundances in megacrysts and their host basalts: Constraints on partition coefficients and megacryst genesis. Geochimica et Cosmochimica Acta, 48, 1201-1221.

Kokelaar, B.P., 1983. The mechanism of Surtseyan volcanism. Journal of the Geological Society of London, 140, 939-944.

Kokelaar, B.P., 1986. Magma-water interactions in subaqueous and emergent basaltic volcanism. Bulletin de Volcanologie, 48, 275-289.

Leake, B.E., Woolley, A.R., Arps, C.E.S., Birch, W.D., Gilbert, M.C., Grice, J.D., Hawthorne, F.C., Kato, A., Kisch, H.J., Krivovichev, V.G., Linthout, K., Laird, J., Mandarino, J.A., Maresch, W.V., Nickel, E.H., Rock, N.M.S., Schumacher, J.C., Smith, D.C., Stephenson, N.C.N., Ungaretti, L., Whittaker, E.J.W., Youzhi, G., 1997. Nomenclature of amphiboles: Report of the Subcommittee on Amphiboles of the International Mineralogical Association, commission on new minerals and mineral names. The Canadian Mineralogist, 35, 219-246.

Le Bas, M.J., Le Maitre, R.W., Streckeisen, A., Zanettin, B., 1986. A chemical classification of volcanic rocks based on the total alkali-silica diagram. Journal of Petrology, 27, 745-750.

Litasov K.D., Foley, S.F., Litasov, Y.D., 2000. Magmatic modification and metasomatism of the subcontinental mantle beneath the Vitim volcanic field (East Siberia): evidence from trace element data on pyroxenite and peridotite xenoliths from Miocene picrobasalt. Lithos, 54, 83-114.

Machado, F., Parsons, W.H., Richards, A.F., Mulford, J.W., 1962. Capelinhos eruption of Fayal volcano, Azores, 1957-1958. Journal of Geophysical Research, 67, 3519-3529.

Menichetti, M., Lodolo, E., Tassone, A., 2008. Structural geology of the Fuegian Andes and Magallanes fold-and-thrust belt –Tierra del Fuego Island. Geologica Acta, 6(1), 19-42.

Moore, J.G., 1985. Structure and eruptive mechanism at Surtsey Volcano, Iceland. Geological Magazine, 122, 649-661.

Morimoto, N., Fabriès, J., Ferguson, A.K., Ginzburg, I.V., Roos, M., Seifert, F.A., Zussman, J., Aoki, K., Gotardi, G., 1988. Nomenclature of pyroxenes. American Mineralogist, 73, 1123-1133.

Pankhurst, R.J., Leat, P.T., Sruoga, P., Rapela, C.W., Márquez, M., Storey, B.C., Riley, T.R., 1998. The Chon-Aike province of Patagonia and related rocks in West Antarctica: a silicic large igneous province. Journal of Volcanology and Geothermal Research, 81, 113-136.

Pankhurst, R.J., Riley, T.R., Fanning, C.M., Kelley, S.P., 2000. Episodic silicic volcanism in Patagonia and the Antarctic Penin-

sula: chronology of magmatism associated with the break-up of Gondwana. Journal of Petrology, 41, 605-625.

Pankhurst, R.J., Hervé, F., Fanning, M., Suárez, M., 2003. Coeval plutonic and volcanic activity in the Patagonian Andes: The Patagonian Batholith and the Ibáñez and Divisadero Formations, Aisén, southern Chile. In: Congreso Geológico Chileno N°10, Concepción, editorial Actas (CD).

Pearce, N.J., Perkins, W.T., Westgate, J.A., Gorton, M.P., Jackson, S.E., Neal, C.R., Chenery, S.P., 1997. A compilation of new and published major and trace element data for NIST SRM 610 and NIST SRM 612 glass reference materials. Geostandards Newsletter, 21, 115-144.

Peterson, R., Francis, D., 1977. The origin of sulphide inclusions in pyroxene megacrysts. American Mineralogist, 62, 1049-1051.

Ramos, V., Aguirre-Urreta, M.B., 1994. Cretaceous evolution of the Magallanes basin. In: Salfity, J.A. (ed.). Cretaceous Tectonics of the Andes. Earth Evolution Series, Fried, Vieweg and Sohn, Braunschweig/Wiesbaden, 315-345.

Rapela, C.W., Pankhurst, R.J., Fanning, C.M., Hervé, F., 2005. Pacific subduction coeval with the Karoo mantle plume: the Early Jurassic Subcordilleran belt of northwestern Patagonia. Geological Society of London, 246(Special Publication), 217-239.

Righter, K., Carmichael, I.S.E., 1993. Mega-xenocrysts in alkali olivine basalts: fragments of disrupted mantle assemblages. American Mineralogist, 78, 1230-1245.

Rossello, E.A., Haring, C.E., Cardinali, G., Suárez, F., Laffitte, G.A., Nevistic, A.V., 2008. Hydrocarbons and petroleum geology of Tierra del Fuego, Argentina. Geologica Acta, 6(1), 69-83.

Schmidt, R., Schmincke, H-U., 2002. From seamount to oceanic island, Porto Santo, central East-Atlantic. International Journal of Earth Sciences (Geologische Rundschau), 91, 594-614.

Shaw, C.S.J., 1997. Origin of sulfide blebs in variably metasomatized mantle xenoliths, Quaternary west Eifel volcanic field, Germany. Canadian Mineralogist, 35, 1453-1463.

Shaw, C.S.J., Eyzaguirre, J., 2000. Origin of megacrysts in the mafic alkaline lavas of the West Eifel volcanic field, Germany. Lithos, 50, 75-95.

Sheridan, M.F., Wohletz, K.H., 1983. Hydrovolcanism: basic considerations and review. Journal of Volcanology and Geothermal Research, 17, 1-29.

Smellie, J.L., Millar, I.L., Rex, D.C., Butterworth, P.J., 1998. Subaqueous basaltic lava dome and carapace breccia on King George Island, South Shetland Islands, Antarctica. Bulletin of Volcanology, 59, 245-261.

Sohn, Y.W., 1996. Hydrovolcanic processes forming basaltic tuff rings and cones on Cheju Island, Korea. Geological Society of America Bulletin, 108, 1199-1211.

Solgevik, H., Mattsson, H.B., Hermelin O., 2007. Growth and emergent tuff cone: Fragmentation and depositional processes recorded in the Capelas tuff cone, São Miguel, Azores. Journal of Volcanology and Geothermal Research, 159, 246-266.

Suárez, M., De la Cruz, R., 2000. Tectonics in the eastern central Patagonian Cordillera (45°30'-47°30'S). Journal of the Geological Society of London, 157, 995-2001.

Suárez, M., De la Cruz, R., Bell, M., 1996. Estratigrafía de la región de Coyhaique (latitud 45°-46°S); Cordillera Patagónica, Chile. Buenos Aires. Congreso Geológico Argentino N° 13 y Congreso de Exploración de Hidrocarburos N° 2, 1(Actas), 575-590.

Suárez, M., De la Cruz, R., Bell, M., 2007. Geología del área Ñireguao-Baño Nuevo, Región Aisén del General Carlos Ibáñez del Campo. Servicio Nacional de Geología y Minería, Carta Geológica de Chile, Serie Geología Básica 1:100.000 Santiago, 108, 56pp.

Suárez, M., Demant, A., De la Cruz, R., Fanning, M., 2010. ^{40}Ar/^{39}Ar and U-Pb SHRIMP dating of Aptian tuff cones in the Aisén basin, Central Patagonian Cordillera. Journal of South American Earth Sciences, 29, 731-737.

Sun, S.S., McDonough, W.F., 1989. Chemical and isotopic systematics of oceanic basalts: implications for mantle composition and processes. In: Saunders, A.D., Norry, M.J. (eds.). Magmatism in Ocean Basins. Geological Society of London, 42(Special Publication), 313-345.

Szabó, C., Bodnar, R.J., 1995. Chemistry and origin of mantle sulfides in spinel peridotite xenoliths from alkaline basaltic lavas, Nógrád-Gömör volcanic field, northern Hungary and southern Slovakia. Geochimica et Cosmochimica Acta, 59, 3917-3927.

Thorarinsson, S., Einarsson, Th., Sigvaldason, G., Elisson, G., 1964. The submarine eruption off the Vestmann Islands 1963–64, a preliminary report. Bulletin de Volcanologie, 27, 435-445.

Tschernich, R.W., 1992. Zeolites of the World. Phoenix (Arizona), Geoscience Press, 563pp.

Waters, A.C., Fisher, R.V., 1971. Base surges and their deposits: Capelinhos and Taal Volcanoes. Journal of Geophysical Research, 76, 5596-5614.

Wilshire, H.G., McGuire, A.V., Noller, J.S., Turrin, B.D., 1991. Petrology of lower crustal and upper mantle xenoliths from the Cima volcanic field, California. Journal of Petrology, 32, 169-200.

Wohletz, K.H., Sheridan, M.F., 1983. Hydrovolcanic explosions II. Evolution of basaltic tuff rings and tuff cones. American Journal of Science, 283, 385-413.

Woodland, A.B., Jugo, P.J., 2007. A complex magmatic system beneath the Devès volcanic field, Massif Central, France: evidence from clinopyroxene megacrysts. Contributions to Mineralogy and Petrology, 153, 719-731.

Zack, T., Foley, S.F., Jenner, G.A., 1997. A consistent partition coefficient set for clinopyroxene, amphibole and garnet from laser ablation microprobe analyses of garnet pyroxenites from Kakanui, New Zealand. Neues Jahrbuch für Mineralogie Abhandlungen, 172, 23-41.

Zajacz, Z., Szabó, C., 2003. Origin of sulphide inclusions in cumulate xenoliths from Nógrád-Gömör volcanic field, Pannonian Basin (north Hungary/south Slovakia). Chemical Geology, 194, 105-117.